

Nodal Topological Superconductivity Driven by Crystalline Antiunitary Symmetry in Altermagnets

Xiao Xiao^{1,2} and Arun Bansil^{1,2}

¹*Department of Physics, Northeastern University, Boston, Massachusetts 02115, USA*

²*Quantum Materials and Sensing Institute, Northeastern University, Burlington, Massachusetts 01803, USA*

Topological superconductivity hosts protected quasiparticles and is central to topological quantum computation, yet its realization in intrinsic materials remains challenging and often relies on engineered platforms. Here we uncover a symmetry-constrained mechanism for nodal topological superconductivity in altermagnets. Focusing on fourfold rotational collinear altermagnets, we show that the native crystalline antiunitary symmetry \mathcal{TC}_{4z} generically forbids pure spin-singlet pairing and selects pairing structures that admit Bogoliubov-de Gennes (BdG) Hamiltonians with emergent chiral symmetries. These symmetries further give rise to robust nodal topological phases over broad parameter regimes, including a nodal-point phase hosting Majorana flat bands (MFBs) and two distinct nodal-loop phases with chiral Majorana edge states. Notably, the nodal structure persists even after spontaneous breaking of the antiunitary symmetry, indicating that the topology originates from symmetry-constrained pairing rather than direct symmetry protection. Finally, we propose tunneling signatures that can distinguish these nodal phases and probe symmetry breaking experimentally.

Introduction. Symmetry fundamentally constrains superconducting pairing states [1, 2], dictating the allowed pairing channels and their topologies. Realizing topological superconductivity therefore requires symmetry settings that enable nontrivial Bogoliubov-de Gennes (BdG) topology [3]. However, most existing routes rely on strong spin-orbit coupling (SOC) [4–6], engineered heterostructures [7–10], or fine-tuned symmetry breaking [11, 12], often requiring delicate tuning and limiting intrinsic material realizations.

Altermagnets (AMs), a recently identified class of magnetic systems [13–15], provide a distinct symmetry setting and host a broad range of emergent properties, including topological and correlated phenomena [10, 16–25], unconventional transport responses [26–50], and spintronic applications [51–56]. Despite a vanishing net magnetization, they exhibit momentum-dependent spin splitting governed by spin-space symmetries tied to the underlying lattice, even in the absence of SOC. Moreover, AMs can host crystalline antiunitary symmetries, formed by combining time-reversal \mathcal{T} with spatial operations, arising from the interplay between spin and lattice degrees of freedom [57–59]. These unconventional symmetry structures, together with momentum-dependent spin splitting, raise the question of how they constrain superconducting pairing and topology [60–71].

Here we uncover a symmetry-driven mechanism for nodal topological superconductivity arising from the crystalline antiunitary symmetry \mathcal{TC}_{4z} in collinear AMs. Group-theoretical analysis reveals that \mathcal{TC}_{4z} admits two irreducible representations (IRRs) for pairing channels: those in the trivial IRR preserve the symmetry, whereas those in the nontrivial IRR spontaneously break it.

We analyze the pairing energetics using linearized gap equations with on-site and nearest-neighbor interactions. A key consequence of symmetry and pairing interactions

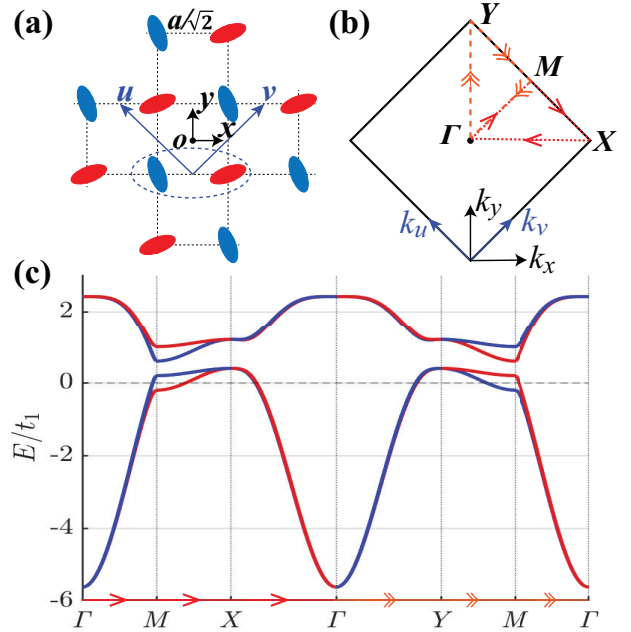


FIG. 1. Normal-state properties: (a) lattice structure; (b) Brillouin zone in which a high-symmetry momentum path is shown; (c) Band structure along the path in (b) with chemical potential $\mu = 0$. In (c), red (blue) curves denote spin-up (spin-down) bands. The hopping parameters are $t_2 = 0.3t_1$, $t_3 = 0.05t_1$, $t_4 = 0.1t_1$, $t_5 = 0.02t_1$, and $J = 0.4t_1$.

is the generic mixing between spin-singlet and spin-triplet components along the spin-quantization axis. We find that the leading pairing channels give rise to BdG Hamiltonians with emergent global chiral symmetries, which stabilize nodal topological superconductivity over broad parameter regimes. For moderate interaction strengths, the system hosts either a nodal-point phase characterized by nontrivial winding numbers or a nodal-loop phase

IRR	W	singlet $\psi(\mathbf{k})(i\sigma_y)$	triplet $(\mathbf{d}(\mathbf{k}) \cdot \boldsymbol{\sigma})(i\sigma_y)$
Γ_1	$ \mathcal{U} $	$\psi_{0;0n}^{\Gamma_1} = f_{0;0}^{\Gamma_1}\tau_0 + f_{0;z}^{\Gamma_1}\tau_z$ $\psi_0^{\Gamma_1}(\mathbf{k}) = C_0^{\Gamma_1}(\mathbf{k})\tau_x$	$d_{z,1}^{\Gamma_1}(\mathbf{k}) = C_{z,1}^{\Gamma_1}(\mathbf{k})\tau_y$ $d_{\pm}^{\Gamma_1}(\mathbf{k}) = iS_{\pm}^{\Gamma_1}(\mathbf{k})\tau_x$
Γ_2	$- \mathcal{U} $	$\psi_{0,1}^{\Gamma_2}(\mathbf{k}) = S_0^{\Gamma_2}(\mathbf{k})(i\tau_y)$	$d_{z,1}^{\Gamma_2}(\mathbf{k}) = iS_{z,1}^{\Gamma_2}(\mathbf{k})\tau_x$ $d_{\pm,1}^{\Gamma_2}(\mathbf{k}) = C_{\pm,1}^{\Gamma_2}(\mathbf{k})\tau_y$

TABLE I. Pairing functions forming bases closed under the antiunitary symmetry \mathcal{TC}_{4z} . The structure factors are $C_m^\Gamma(\mathbf{k}) = f_{m;x}^\Gamma \cos \frac{k_x}{\sqrt{2}} + f_{m;y}^\Gamma \cos \frac{k_y}{\sqrt{2}}$ and $S_m^\Gamma(\mathbf{k}) = f_{m;x}^\Gamma \sin \frac{k_x}{\sqrt{2}} + f_{m;y}^\Gamma \sin \frac{k_y}{\sqrt{2}}$, where $m = 0, z, \pm$ label the singlet, z -component triplet, and \pm -component triplet channels. The relation between $f_{m;x}^\Gamma$ and $f_{m;y}^\Gamma$ depends on whether \mathcal{TC}_{4z} is preserved or broken. For Γ_2 , the doubled components are omitted for clarity and can be generated by applying \mathcal{TC}_{4z} to $\psi_1(\mathbf{k})$, $d_{z,1}(\mathbf{k})$, and $d_{\pm,1}(\mathbf{k})$.

protected by \mathbb{Z}_2 invariants, depending on the chemical potential. In the nodal-point phase, the chiral symmetry enforces zero-energy boundary states, giving rise to Majorana flat bands (MFBs) [72, 73]. At stronger interactions, a nodal-loop phase that spontaneously breaks \mathcal{TC}_{4z} can also emerge, with topology likewise characterized by \mathbb{Z}_2 invariants. Finally, we demonstrate distinct tunneling signatures that distinguish these nodal phases and diagnose whether the antiunitary symmetry is preserved or spontaneously broken.

Model of the AM normal state. A generic fourfold rotational collinear AM with \mathcal{TC}_{4z} symmetry can be realized on a two-sublattice square lattice [Fig. 1(a)], with the corresponding Brillouin zone shown in Fig. 1(b). With Pauli matrices τ_i and σ_i acting on sublattice and spin spaces, the normal-state Hamiltonian, including hopping up to the third-nearest-neighbor sites, is

$$\mathcal{H}(\mathbf{k}) = -c_1(\mathbf{k})\tau_x\sigma_0 - c_2(\mathbf{k})\tau_0\sigma_0 + c_3(\mathbf{k})\tau_z\sigma_0 + J\tau_z\sigma_z, \quad (1)$$

where $c_1 = 2t_1(\cos \frac{k_x}{\sqrt{2}} + \cos \frac{k_y}{\sqrt{2}})$, $c_2 = 4t_2 \cos \frac{k_x}{\sqrt{2}} \cos \frac{k_y}{\sqrt{2}} + 2t_4(\cos \sqrt{2}k_x + \cos \sqrt{2}k_y)$, and $c_3 = 4t_3 \sin \frac{k_x}{\sqrt{2}} \sin \frac{k_y}{\sqrt{2}} + 2t_5(\cos \sqrt{2}k_x - \cos \sqrt{2}k_y)$. We set the primitive lattice constant to $a = 1$. The c_3 term breaks mirror symmetries of the square lattice, leaving \mathcal{TC}_{4z} as the only remaining symmetry. The band structure along the high-symmetry path marked in Fig. 1(b) is shown in Fig. 1(c), where the characteristic momentum-dependent spin splitting of altermagnets is clearly visible.

Pairing channels constrained by \mathcal{TC}_{4z} . The allowed superconducting pairing channels are constrained by the symmetry group \mathcal{G} generated by \mathcal{TC}_{4z} . This group can be decomposed as $\mathcal{G} = \mathcal{U} \oplus \mathcal{TC}_{4z}\mathcal{U}$, where \mathcal{U} is the unitary subgroup generated by $g_1 = (\mathcal{TC}_{4z})^2$. Since \mathcal{U} is isomorphic to the cyclic group $C_4 = \{e, g_1, g_1^2, g_1^3\}$, it admits four IRRs.

To classify pairing channels according to these IRRs,

we construct the projection operator

$$P^{\Gamma_n} = \frac{1}{|\mathcal{U}|} \sum_{g_j \in \mathcal{U}} \chi^{\Gamma_n}(g_j)^* D(g_j), \quad (2)$$

where $|\mathcal{U}|$ is the order of \mathcal{U} , Γ_n labels the IRR, $\chi^{\Gamma_n}(g_j)$ is the corresponding character, and $D(g_j)$ is the representation acting on Bloch states. Applying the projectors yields pairing functions for each IRR of \mathcal{U} .

In the presence of the antiunitary symmetry, the pairing functions for \mathcal{G} are obtained from those of \mathcal{U} via the Wigner test [74],

$$W = \sum_{g_j \in \mathcal{U}} \chi^{\Gamma_n}((\mathcal{TC}_{4z}g_j)^2). \quad (3)$$

If $W = |\mathcal{U}|$, the pairing functions of \mathcal{U} directly furnish those of \mathcal{G} . If $W = -|\mathcal{U}|$ or $W = 0$, the representation is doubled by including the action of \mathcal{TC}_{4z} on the pairing functions of \mathcal{U} .

Assuming pairing up to nearest neighbors, a straightforward analysis shows that the pairing functions in two of the four IRRs vanish, while those in the remaining two IRRs are summarized in Table I. Since these pairing functions form a complete basis, the gap function can be expanded accordingly and recast in terms of an orthonormal basis $\{\Psi_{m;a}^\Gamma(\mathbf{k})\}$ (see Supplemental Material for details [75]) as

$$\Delta(\mathbf{k}) = D_0 \left[\eta_{0;0}^{\Gamma_1} \Psi_{0;0}^{\Gamma_1} + \eta_{0;z}^{\Gamma_1} \Psi_{0;z}^{\Gamma_1} + \sum'_{\Gamma, m, a} \eta_{m;a}^{\Gamma} \Psi_{m;a}^{\Gamma}(\mathbf{k}) \right], \quad (4)$$

where the first two on-site pairing terms are written separately from the primed nearest-neighbor summation; $\Gamma \in \{\Gamma_1, \Gamma_2\}$ labels the IRR, $m \in \{0, z, \pm\}$ the pairing channel, and $a \in \{x, y\}$ the component index; the coefficients $\eta_{m;a}^\Gamma$ denote the corresponding order parameters, and D_0 , taken as $0.1t_1$ throughout this work, sets the overall superconducting gap scale.

Mixing of singlet and z -component triplet. To identify generic energetic constraints, we expand the interaction in the pairing basis as [76, 77]:

$$V(\mathbf{k}, \mathbf{k}') = -V_0 \left[\Psi_{0,0}^{\Gamma_1}(\mathbf{k}) \Psi_{0,0}^{\Gamma_1}(\mathbf{k}')^\dagger + \Psi_{0,z}^{\Gamma_1}(\mathbf{k}) \Psi_{0,z}^{\Gamma_1}(\mathbf{k}')^\dagger \right] - V_1 \sum'_{\Gamma, m, a} \Psi_{m;a}^{\Gamma}(\mathbf{k}) \Psi_{m;a}^{\Gamma}(\mathbf{k}')^\dagger, \quad (5)$$

where V_0 and V_1 denote the coupling strengths for the on-site and nearest-neighbor channels, respectively. Near the superconducting onset, the gap function is small, and the self-consistent gap equation can be linearized to yield

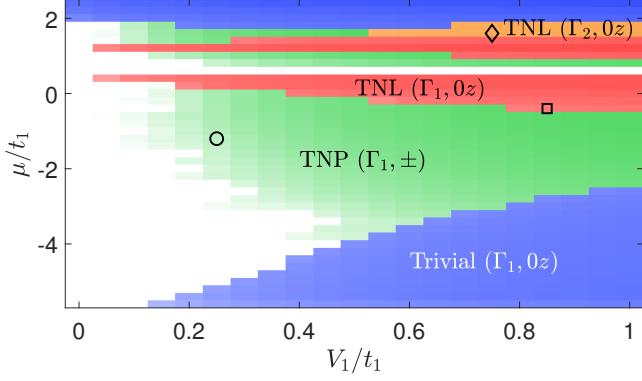


FIG. 2. Phase diagram of the leading superconducting instability for the model with \mathcal{TC}_{4z} as a function of μ and V_1 , with $V_0/t_1 = 0.5$. Colors denote different leading pairing phases, while brightness encodes the magnitude of T_c . The lowest visible value is $k_B T_c/t_1 = 10^{-6}$.

(see Supplemental Material for details [75]):

$$\eta_{m,a}^\Gamma = V_{m,a}^\Gamma k_B T \sum_{\Gamma', m', a'} \eta_{m', a'}^{\Gamma'} \times \sum_{\mathbf{k}', n} \text{Tr} \left[\Psi_{m,a}^\Gamma(\mathbf{k}')^\dagger \mathcal{G}_{\mathbf{k}'}(i\omega_n) \Psi_{m', a'}^{\Gamma'}(\mathbf{k}') \bar{\mathcal{G}}_{-\mathbf{k}'}(i\omega_n) \right], \quad (6)$$

where $V_{m,a}^\Gamma = V_0$ for $(\Gamma, m, a) = (\Gamma_1, 0, 0)$ or $(\Gamma_1, 0, z)$, and $V_{m,a}^\Gamma = V_1$ otherwise. Here $\mathcal{G}_{\mathbf{k}'}$ and $\bar{\mathcal{G}}_{-\mathbf{k}'}$ denote the normal-state Matsubara Green's functions for electrons and holes, respectively.

For a collinear alternating normal state, the spin sector of the Green's functions can be separated and has the form $P_s = (\sigma_0 + s\sigma_z)/2$ with $s = \pm 1$. The spin structures of the pairing channels are $i\sigma_y$ for the singlet ($m = 0$) and $\sigma_z(i\sigma_y)$ for the z -component of the triplet ($m = z$). Consequently, $\text{Tr}[(i\sigma_y)P_s \sigma_z(i\sigma_y)P_{s'}]$ is nonzero whenever $s \neq s'$. This implies that, in collinear alternating magnets, the singlet channel generically mixes with the z -component of the triplet channel, constituting the first key result of this work.

Phase diagram. From Eq. (6), we determine the phase diagram of the leading pairing instabilities, characterized by T_c , in the (μ, V_0, V_1) parameter space. A representative phase diagram for $V_0/t_1 = 0.5$ is shown in Fig. 2. At the bottom and top of the bands (blue regions), the singlet-triplet mixed $0z$ channel in Γ_1 dominates. Owing to dominant on-site pairing components, these phases are trivial and fully gapped. However, between the two trivial regions, three distinct topological nodal phases emerge over a broad parameter range, which we discuss below.

Topological nodal-point superconductivity and MFBs. In the green regions of Fig. 2, the $+$ and $-$ triplet pairing channels in Γ_1 are degenerate at the leading instability. The \mathcal{TC}_{4z} symmetry further constrains the order

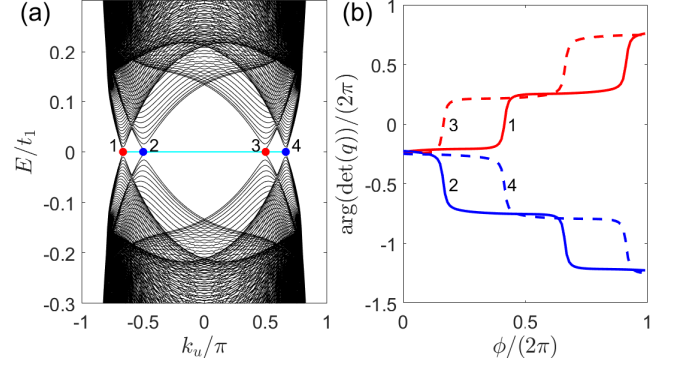


FIG. 3. Topological nodal-point superconducting phase: (a) Low-energy spectrum of a finite-size system with $L = 500a$ as a function of k_u , with edge states highlighted in cyan. The four dots denote the projections of the bulk nodal points onto the k_u axis; red (blue) dots correspond to nodes with winding number $\nu = 1$ ($\nu = -1$). (b) Phase winding of $\det[q(\mathbf{k})]$ around the four nodal points, evaluated along closed loops encircling each.

parameters as $\eta_{+,x}^{\Gamma_1} = \pm i(\eta_{-,y}^{\Gamma_1})^*$ and $\eta_{+,y}^{\Gamma_1} = \mp i(\eta_{-,x}^{\Gamma_1})^*$. As a result, the BdG Hamiltonian exhibits a global chiral symmetry $\mathcal{C} = \kappa_y \otimes \tau_0 \otimes P_{s=+1} + \kappa_x \otimes \tau_0 \otimes P_{s=-1}$, where κ_i are Pauli matrices in Nambu space and $P_{s=\pm 1}$ are the spin projectors defined below Eq. (6). In the chiral basis of \mathcal{C} , the Hamiltonian takes an off-diagonal form with blocks $q(\mathbf{k})$ and $q^\dagger(\mathbf{k})$.

Since $\det(q(\mathbf{k}))$ is generally complex, the nodal condition requires both $\Re[\det(q(\mathbf{k}))] = 0$ and $\Im[\det(q(\mathbf{k}))] = 0$. In two dimensions, these two constraints generically yield isolated solutions, corresponding to geometrically stable nodal points. The complex $\det(q(\mathbf{k}))$ exhibits a non-trivial winding around these nodes, endowing them with topological protection characterized by a winding number ν . These features are confirmed in Fig. 3 at a representative parameter point (denoted by the circle in Fig. 2). Crucially, in this phase \mathcal{C} is preserved locally at each \mathbf{k} , rather than only globally through the BdG relation between \mathbf{k} and $-\mathbf{k}$, thereby pinning the boundary spectrum to zero energy and giving rise to MFBs.

Topological nodal-loop superconductivity. In the red regions of Fig. 2, Eq. (6) selects a state with vanishing $\eta_{0;0}^{\Gamma_1}$ and finite $\eta_{0;z}^{\Gamma_1}$. The \mathcal{TC}_{4z} symmetry further constrains the order parameters to be purely imaginary, such that $\eta_{0;a}^{\Gamma_1} = \pm(\eta_{0;a}^{\Gamma_1})^*$ and $\eta_{z;a}^{\Gamma_1} = \pm(\eta_{z;a}^{\Gamma_1})^*$. The resulting BdG Hamiltonian possesses a global chiral symmetry generated by κ_x . In addition, an emergent antiunitary symmetry $\mathcal{A} = \kappa_z K$, with K denoting complex conjugation, enforces the off-diagonal block $q(\mathbf{k})$ to be real. Consequently, the nodal structure is determined solely by $\Re \det[q(\mathbf{k})] = 0$. In two dimensions, this single constraint generically gives rise to geometrically stable nodal loops. Their topology is characterized by a \mathbb{Z}_2 invariant given by $\text{sgn}[\det(q)]$, which supports topologically pro-

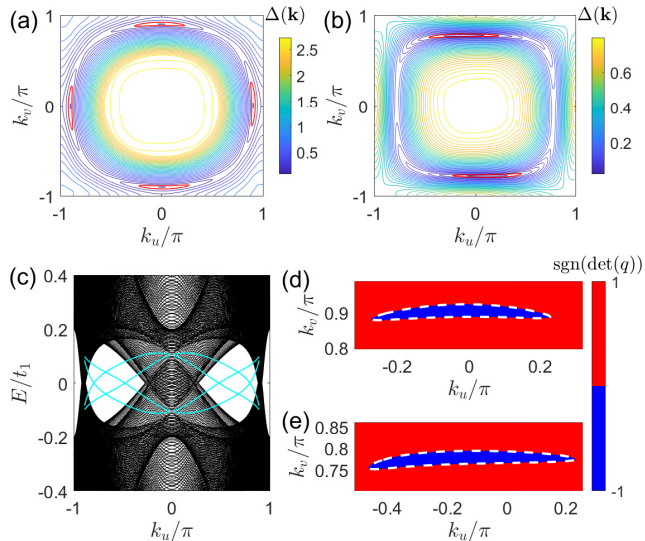


FIG. 4. Topological nodal-loop superconducting phases: (a,b) Gap distributions in the Brillouin zone for the $0z$ channels in Γ_1 and Γ_2 , respectively, with nodal loops highlighted in red. (c) Low-energy spectrum of a finite-size system ($L = 500a$) as a function of k_u in the Γ_1 TNL phase, with edge states highlighted in cyan. (d,e) \mathbb{Z}_2 topology of the nodal loops, revealed by the sign of $\det(q)$ along representative loops (white dashed curves) for the TNL phases in Γ_1 and Γ_2 , respectively.

tected chiral edge states.

In the orange region of Fig. 2, the leading instability corresponds to the $0z$ channel in Γ_2 . In this case, \mathcal{TC}_{4z} enforces the corresponding order parameters to vanish, so the selection of this phase by Eq. (6) spontaneously breaks \mathcal{TC}_{4z} . From the resulting order parameters, we again identify a chiral symmetry generated by κ_y , together with an emergent antiunitary symmetry $\mathcal{A} = (\kappa_z \otimes u)K$ with $u = \text{diag}(1, -1, 1, -1)$, which similarly constrains $q(\mathbf{k})$ to be real. Consequently, the system also realizes a topological nodal-loop superconducting phase, but with \mathcal{TC}_{4z} spontaneously broken.

The numerical results in Fig. 4 at two representative parameter points (denoted by square and diamond symbols in Fig. 2) corroborate this analysis. In the Γ_1 phase, the preservation of \mathcal{TC}_{4z} leads to four symmetry-related nodal loops [Fig. 4(a)], whereas in the Γ_2 phase the spontaneous breaking of \mathcal{TC}_{4z} reduces the nodal structure to two loops [Fig. 4(b)], explicitly breaking fourfold rotational symmetry.

Tunneling fingerprints of the nodal phases. These three topological nodal phases can be distinguished via tunneling spectroscopy in two planar junctions with half-metallic leads [78] related by \mathcal{TC}_{4z} . One configuration has the junction along v with the magnetization in the lead along z , while \mathcal{TC}_{4z} maps it to a second configuration along u with the magnetization along $-z$ (Fig. 5).

In the TNP phase, MFBs induce resonant equal-spin

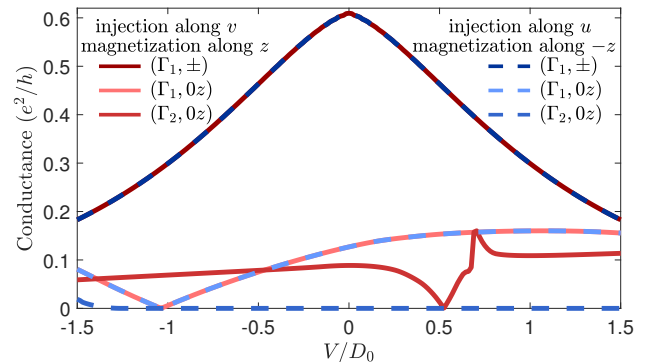


FIG. 5. Tunneling spectra of planar junctions between an altermagnetic superconductor and a half-metallic lead. Solid (dashed) curves correspond to injection along the v (u) direction with the lead spin polarization aligned along z ($-z$). The two configurations are related by \mathcal{TC}_{4z} . Colors distinguish the pairing channels (Γ_1, \pm) , $(\Gamma_1, 0z)$, and $(\Gamma_2, 0z)$.

Andreev reflection [79], yielding a pronounced zero-bias conductance peak. In contrast, for the TNL phases in the $0z$ channel, Andreev reflection is forbidden for z -polarized half-metal leads, so low-energy transport is dominated by quasiparticle tunneling and the conductance is strongly suppressed.

Both the TNP phase and the TNL phase in Γ_1 preserve \mathcal{TC}_{4z} , leading to identical spectra for the two configurations. By contrast, in the Γ_2 TNL phase, the spontaneous breaking of \mathcal{TC}_{4z} results in distinct tunneling spectra.

Influence of SOC. We have focused on the spin-conserving limit in which the nodal phases are protected by chiral and/or real symmetries. In the presence of SOC, these protecting symmetries might be broken [80]. In these cases, the nodal structures become fully gapped but may still realize distinct topological superconducting states [3]. In particular, upon gapping, the system may have a nonzero Chern number and realize a chiral topological superconducting phase [61, 81]. Moreover, in the present model, the interplay between SOC-induced mass terms and the underlying rotational structure naturally leads to edge-dependent mass configurations, in which the mass acquires different signs on edges related by rotation. This provides a natural route to a higher-order topological superconducting phase, characterized by domain walls at the corners and the emergence of Majorana zero modes [61]. The absence of mirror and inversion symmetries further removes constraints that would otherwise enforce cancellation of topological contributions [82, 83], making the emergence of chiral or higher-order topology a natural consequence once SOC gaps the nodal phases¹.

¹ A detailed investigation of these possibilities would be interesting, but it is beyond the scope of this work.

Material realizations. A relevant materials context for the present model can be identified from two complementary directions. First, recent classifications of two-dimensional altermagnets [84] have identified candidate materials with spin groups containing $4'$ (equivalent to \mathcal{TC}_{4z}), such as V_2Se_2O [26], V_2Te_2O [27], and Cr_2O_2 [28, 29]. These systems already realize the key symmetry underlying our model, although they typically possess additional crystalline symmetries. In practice, such additional symmetries may obscure the minimal symmetry setting considered here, but can be selectively reduced, for example, by substrate effects [85] or strain [86], thereby bringing the system closer to the \mathcal{TC}_{4z} limit.

A complementary route is provided by quasi-two-dimensional organic charge-transfer salts such as κ -Cl [20]. These systems realize correlated electrons on an anisotropic triangular lattice characterized by hopping amplitudes t and t' , and therefore do not possess the \mathcal{TC}_{4z} assumed here. However, their electronic structure might be continuously tuned through pressure, chemical substitution, or molecular engineering [87, 88], which modify the ratio t'/t . In the limit $t'/t \rightarrow 1$, the lattice approaches a square geometry, and the system moves toward the \mathcal{TC}_{4z} symmetry regime.

Our work therefore isolates the essential role of \mathcal{TC}_{4z} and explores a reduced symmetry setting that may be approached either by symmetry reduction in $4'$ -symmetric materials or by lattice tuning in organic systems.

Conclusions. We have demonstrated that in a collinear altermagnetic system with \mathcal{TC}_{4z} symmetry, the crystalline antiunitary symmetry, in conjunction with the altermagnetic spin structure, plays a central role in stabilizing distinct nodal topological superconducting phases. Importantly, these phases emerge naturally from symmetry and are robust over broad parameter regimes, enhancing their experimental accessibility. We further show that they exhibit distinct and experimentally accessible signatures in tunneling spectroscopy, providing a direct route for their detection. Our results establish a symmetry-based framework for realizing topological superconductivity in altermagnetic systems and open a pathway toward robust topological superconductivity beyond conventional symmetry settings.

Acknowledgment. This work was supported by the National Science Foundation through the Expand-QISE award NSF-OMA-2329067 and benefited from the resources of Northeastern University's Advanced Scientific Computation Center, the Discovery Cluster, the Massachusetts Technology Collaborative award MTC-22032, and the Quantum Materials and Sensing Institute.

[1] M. Sigrist and K. Ueda, Phenomenological theory of unconventional superconductivity, *Rev. Mod. Phys.* **63**, 239

- (1991).
- [2] V. P. Mineev and K. V. Samokhin, *Introduction to Unconventional Superconductivity* (Gordon and Breach Science Publishers, Amsterdam, 1999).
- [3] M. Sato and Y. Ando, Topological superconductors: a review, *Reports on Progress in Physics* **80**, 076501 (2017).
- [4] J. Alicea, New directions in the pursuit of majorana fermions in solid state systems, *Reports on Progress in Physics* **75**, 076501 (2012).
- [5] F. Pientka, A. Keselman, E. Berg, A. Yacoby, A. Stern, and B. I. Halperin, Topological superconductivity in a planar josephson junction, *Phys. Rev. X* **7**, 021032 (2017).
- [6] H. Ren, F. Pientka, S. Hart, A. T. Pierce, M. Kosowsky, L. Lunczer, R. Schlereth, B. Scharf, E. M. Hankiewicz, L. W. Molenkamp, B. I. Halperin, and A. Yacoby, Topological superconductivity in a phase-controlled josephson junction, *Nature* **569**, 93–98 (2019).
- [7] R. M. Lutchyn, E. P. A. M. Bakkers, L. P. Kouwenhoven, P. Krogstrup, C. M. Marcus, and Y. Oreg, Majorana zero modes in superconductor–semiconductor heterostructures, *Nature Reviews Materials* **3**, 52–68 (2018).
- [8] R. M. Lutchyn, J. D. Sau, and S. Das Sarma, Majorana fermions and a topological phase transition in semiconductor-superconductor heterostructures, *Phys. Rev. Lett.* **105**, 077001 (2010).
- [9] Y. Oreg, G. Refael, and F. von Oppen, Helical liquids and majorana bound states in quantum wires, *Phys. Rev. Lett.* **105**, 177002 (2010).
- [10] S. A. A. Ghorashi, T. L. Hughes, and J. Cano, Altermagnetic routes to majorana modes in zero net magnetization, *Phys. Rev. Lett.* **133**, 106601 (2024).
- [11] F. Pientka, L. I. Glazman, and F. von Oppen, Topological superconducting phase in helical shiba chains, *Phys. Rev. B* **88**, 155420 (2013).
- [12] S. Nadj-Perge, I. K. Drozdov, J. Li, H. Chen, S. Jeon, J. Seo, A. H. MacDonald, B. A. Bernevig, and A. Yazdani, Observation of majorana fermions in ferromagnetic atomic chains on a superconductor, *Science* **346**, 602–607 (2014).
- [13] L. Šmejkal, R. Gonzalez-Hernandez, T. Jungwirth, and J. Sinova, Crystal time-reversal symmetry breaking and spontaneous Hall effect in collinear antiferromagnets, *Sci. Adv.* **6**, eaaz8809 (2020).
- [14] L. Šmejkal, J. Sinova, and T. Jungwirth, Beyond conventional ferromagnetism and antiferromagnetism: A phase with nonrelativistic spin and crystal rotation symmetry, *Phys. Rev. X* **12**, 031042 (2022).
- [15] L. Šmejkal, J. Sinova, and T. Jungwirth, Emerging research landscape of altermagnetism, *Phys. Rev. X* **12**, 040501 (2022).
- [16] L. Šmejkal, A. Marmodoro, K.-H. Ahn, R. González-Hernández, I. Turek, S. Mankovsky, H. Ebert, S. W. D'Souza, O. c. v. Šipr, J. Sinova, and T. c. v. Jungwirth, Chiral magnons in altermagnetic ruo_2 , *Phys. Rev. Lett.* **131**, 256703 (2023).
- [17] S. Bhowal and N. A. Spaldin, Ferroically ordered magnetic octupoles in d -wave altermagnets, *Phys. Rev. X* **14**, 011019 (2024).
- [18] P. A. McClarty and J. G. Rau, Landau theory of altermagnetism, *Phys. Rev. Lett.* **132**, 176702 (2024).
- [19] V. Leeb, A. Mook, L. Šmejkal, and J. Knolle, Spontaneous formation of altermagnetism from orbital ordering, *Phys. Rev. Lett.* **132**, 236701 (2024).

- [20] Y. Yu, H. G. Suh, M. Roig, and D. F. Agterberg, Altermagnetism from coincident Van Hove singularities: application to κ -Cl, *Nat. Commun.* **16**, 2950 (2025).
- [21] Y.-X. Li and C.-C. Liu, Majorana corner modes and tunable patterns in an altermagnet heterostructure, *Phys. Rev. B* **108**, 205410 (2023).
- [22] Y.-X. Li, Y. Liu, and C.-C. Liu, Creation and manipulation of higher-order topological states by altermagnets, *Phys. Rev. B* **109**, L201109 (2024).
- [23] R. M. Fernandes, V. S. de Carvalho, T. Birol, and R. G. Pereira, Topological transition from nodal to nodeless zeeman splitting in altermagnets, *Phys. Rev. B* **109**, 024404 (2024).
- [24] D. S. Antonenko, R. M. Fernandes, and J. W. F. Venderbos, Mirror chern bands and weyl nodal loops in altermagnets, *Phys. Rev. Lett.* **134**, 096703 (2025).
- [25] K. Parshukov, R. Wiedmann, and A. P. Schnyder, Topological crossings in two-dimensional altermagnets: Symmetry classification and topological responses, *Phys. Rev. B* **111**, 224406 (2025).
- [26] H.-Y. Ma, M. Hu, N. Li, J. Liu, W. Yao, J.-F. Jia, and J. Liu, Multifunctional antiferromagnetic materials with giant piezomagnetism and noncollinear spin current, *Nat. Commun.* **12**, 2846 (2021).
- [27] Q. Cui, Y. Zhu, X. Yao, P. Cui, and H. Yang, Giant spin-hall and tunneling magnetoresistance effects based on a two-dimensional nonrelativistic antiferromagnetic metal, *Phys. Rev. B* **108**, 024410 (2023).
- [28] X. Chen, D. Wang, L. Li, and B. Sanyal, Giant spin-splitting and tunable spin-momentum locked transport in room temperature collinear antiferromagnetic semimetallic CrO monolayer, *Appl. Phys. Lett.* **123**, 022402 (2023).
- [29] P.-J. Guo, Z.-X. Liu, and Z.-Y. Lu, Quantum anomalous Hall effect in collinear antiferromagnetism, *npj Comput. Mater.* **9**, 70 (2023).
- [30] Q. Cui, B. Zeng, P. Cui, T. Yu, and H. Yang, Efficient spin seebeck and spin nernst effects of magnons in altermagnets, *Phys. Rev. B* **108**, L180401 (2023).
- [31] Y. Fang, J. Cano, and S. A. A. Ghorashi, Quantum geometry induced nonlinear transport in altermagnets, *Phys. Rev. Lett.* **133**, 106701 (2024).
- [32] L. Attias, A. Levchenko, and M. Khodas, Intrinsic anomalous hall effect in altermagnets, *Phys. Rev. B* **110**, 094425 (2024).
- [33] X. Zhou, W. Feng, R.-W. Zhang, L. Šmejkal, J. Sinova, Y. Mokrousov, and Y. Yao, Crystal thermal transport in altermagnetic RuO_2 , *Phys. Rev. Lett.* **132**, 056701 (2024).
- [34] E. Syljuåsen, A. Qaiumzadeh, and A. Sudbø, Quantum geometry and magnon hall transport in an altermagnet, *Phys. Rev. B* **112**, 064429 (2025).
- [35] S.-B. Zhang, L.-H. Hu, and T. Neupert, Finite-momentum cooper pairing in proximitized altermagnets, *Nature Communications* **15**, 1801 (2024).
- [36] C. Sun, A. Brataas, and J. Linder, Andreev reflection in altermagnets, *Phys. Rev. B* **108**, 054511 (2023).
- [37] M. Papaj, Andreev reflection at the altermagnet-superconductor interface, *Phys. Rev. B* **108**, L060508 (2023).
- [38] C. W. J. Beenakker and T. Vakhel, Phase-shifted andreev levels in an altermagnet josephson junction, *Phys. Rev. B* **108**, 075425 (2023).
- [39] J. A. Ouassou, A. Brataas, and J. Linder, dc josephson effect in altermagnets, *Phys. Rev. Lett.* **131**, 076003 (2023).
- [40] B. Lu, K. Maeda, H. Ito, K. Yada, and Y. Tanaka, φ josephson junction induced by altermagnetism, *Phys. Rev. Lett.* **133**, 226002 (2024).
- [41] Q. Cheng and Q.-F. Sun, Orientation-dependent josephson effect in spin-singlet superconductor/altermagnet/spin-triplet superconductor junctions, *Phys. Rev. B* **109**, 024517 (2024).
- [42] M. Wei, L. Xiang, F. Xu, L. Zhang, G. Tang, and J. Wang, Gapless superconducting state and mirage gap in altermagnets, *Phys. Rev. B* **109**, L201404 (2024).
- [43] S. Banerjee and M. S. Scheurer, Altermagnetic superconducting diode effect, *Phys. Rev. B* **110**, 024503 (2024).
- [44] Q. Cheng, Y. Mao, and Q.-F. Sun, Field-free josephson diode effect in altermagnet/normal metal/altermagnet junctions, *Phys. Rev. B* **110**, 014518 (2024).
- [45] D. Chakraborty and A. M. Black-Schaffer, Perfect superconducting diode effect in altermagnets, *Phys. Rev. Lett.* **135**, 026001 (2025).
- [46] G. Sim and J. Knolle, Pair density waves and supercurrent diode effect in altermagnets, *Phys. Rev. B* **112**, L020502 (2025).
- [47] I. d. M. Frolidi and H. Freire, Efficiency of the superconducting diode effect of pair-density-wave states in two-dimensional d-wave altermagnets, *Ann. Phys.* **483**, 170273 (2025).
- [48] I. de M. Frolidi and H. Freire, Highly efficient superconducting diode effect in unconventional p -wave magnets, (2026), [arXiv:2601.09783 \[cond-mat.supr-con\]](https://arxiv.org/abs/2601.09783).
- [49] A. A. Zyuzin, Magnetoelectric effect in superconductors with d -wave magnetization, *Phys. Rev. B* **109**, L220505 (2024).
- [50] J.-X. Hu, O. Matsyshyn, and J. C. W. Song, Nonlinear superconducting magnetoelectric effect, *Phys. Rev. Lett.* **134**, 026001 (2025).
- [51] L. Šmejkal, A. B. Hellenes, R. González-Hernández, J. Sinova, and T. Jungwirth, Giant and tunneling magnetoresistance in unconventional collinear antiferromagnets with nonrelativistic spin-momentum coupling, *Phys. Rev. X* **12**, 011028 (2022).
- [52] H. Bai, Y. C. Zhang, Y. J. Zhou, P. Chen, C. H. Wan, L. Han, W. X. Zhu, S. X. Liang, Y. C. Su, X. F. Han, F. Pan, and C. Song, Efficient spin-to-charge conversion via altermagnetic spin splitting effect in antiferromagnet RuO_2 , *Phys. Rev. Lett.* **130**, 216701 (2023).
- [53] C. Sun and J. Linder, Spin pumping from a ferromagnetic insulator into an altermagnet, *Phys. Rev. B* **108**, L140408 (2023).
- [54] R.-W. Zhang, C. Cui, R. Li, J. Duan, L. Li, Z.-M. Yu, and Y. Yao, Predictable gate-field control of spin in altermagnets with spin-layer coupling, *Phys. Rev. Lett.* **133**, 056401 (2024).
- [55] E. W. Hodt and J. Linder, Spin pumping in an altermagnet/normal-metal bilayer, *Phys. Rev. B* **109**, 174438 (2024).
- [56] B. Chi, L. Jiang, Y. Zhu, G. Yu, C. Wan, J. Zhang, and X. Han, Crystal-facet-oriented altermagnets for detecting ferromagnetic and antiferromagnetic states by giant tunneling magnetoresistance, *Phys. Rev. Appl.* **21**, 034038 (2024).
- [57] Z. Xiao, J. Zhao, Y. Li, R. Shindou, and Z.-D. Song, Spin space groups: Full classification and applications, *Phys. Rev. X* **14**, 031037 (2024).
- [58] X. Chen, J. Ren, Y. Zhu, Y. Yu, A. Zhang, P. Liu, J. Li, Y. Liu, C. Li, and Q. Liu, Enumeration and representa-

- tion theory of spin space groups, *Phys. Rev. X* **14**, 031038 (2024).
- [59] Y. Jiang, Z. Song, T. Zhu, Z. Fang, H. Weng, Z.-X. Liu, J. Yang, and C. Fang, Enumeration of spin-space groups: Toward a complete description of symmetries of magnetic orders, *Phys. Rev. X* **14**, 031039 (2024).
- [60] I. I. Mazin, Notes on altermagnetism and superconductivity, *AAPPS Bull.* **35**, 18 (2025).
- [61] D. Zhu, Z.-Y. Zhuang, Z. Wu, and Z. Yan, Topological superconductivity in two-dimensional altermagnetic metals, *Phys. Rev. B* **108**, 184505 (2023).
- [62] B. Brekke, A. Brataas, and A. Sudbø, Two-dimensional altermagnets: Superconductivity in a minimal microscopic model, *Phys. Rev. B* **108**, 224421 (2023).
- [63] V. S. de Carvalho and H. Freire, Unconventional superconductivity in altermagnets with spin-orbit coupling, *Phys. Rev. B* **110**, L220503 (2024).
- [64] D. Chakraborty and A. M. Black-Schaffer, Constraints on superconducting pairing in altermagnets, *Phys. Rev. B* **112**, 014516 (2025).
- [65] X. Feng and Z. Zhang, Superconducting order parameters in spin space groups: Methodology and application, *Phys. Rev. B* **111**, 054520 (2025).
- [66] K. Parshukov and A. P. Schnyder, Exotic superconducting states in altermagnets, (2025), [arXiv:2507.10700 \[cond-mat.supr-con\]](https://arxiv.org/abs/2507.10700).
- [67] T. F. Heung and M. Franz, Probing topological degeneracy on a torus using superconducting altermagnets, *Phys. Rev. B* **111**, 205145 (2025).
- [68] Y.-M. Wu, Y. Wang, and R. M. Fernandes, Intra-unit-cell singlet pairing mediated by altermagnetic fluctuations, *Phys. Rev. Lett.* **135**, 156001 (2025).
- [69] Y. Fukaya, B. Lu, K. Yada, Y. Tanaka, and J. Cayao, Crossed surface flat bands in three-dimensional superconducting altermagnets, *Phys. Rev. Lett.* (2026).
- [70] X. Zou, R. M. Fernandes, and E. Fradkin, Superconducting states and intertwined orders in metallic altermagnets, (2026), [arXiv:2603.04503 \[cond-mat.supr-con\]](https://arxiv.org/abs/2603.04503).
- [71] X.-J. Luo, Z.-T. Sun, X. Feng, M. Tian, and K. T. Law, Hidden zeeman field in odd-parity magnets: An ideal platform for topological superconductivity, (2026), [arXiv:2603.15147 \[cond-mat.supr-con\]](https://arxiv.org/abs/2603.15147).
- [72] C. L. M. Wong, J. Liu, K. T. Law, and P. A. Lee, Majorana flat bands and unidirectional majorana edge states in gapless topological superconductors, *Phys. Rev. B* **88**, 060504(R) (2013).
- [73] A. Daido and Y. Yanase, Majorana flat bands, chiral majorana edge states, and unidirectional majorana edge states in noncentrosymmetric superconductors, *Phys. Rev. B* **95**, 134507 (2017).
- [74] M. S. Dresselhaus, G. Dresselhaus, and A. Jorio, *Group Theory: Application to the Physics of Condensed Matter* (Springer, 2008).
- [75] See Supplemental Material for additional details.
- [76] J. Goryo, M. H. Fischer, and M. Sigrist, Possible pairing symmetries in srptas with a local lack of inversion center, *Phys. Rev. B* **86**, 100507(R) (2012).
- [77] N. F. Q. Yuan, K. F. Mak, and K. T. Law, Possible topological superconducting phases of mos_2 , *Phys. Rev. Lett.* **113**, 097001 (2014).
- [78] R. S. Keizer, S. T. B. Goennenwein, T. M. Klapwijk, G. Miao, G. Xiao, and A. Gupta, A spin triplet supercurrent through the half-metallic ferromagnet cro_2 , *Nature* **439**, 825 (2006).
- [79] J. J. He, T. K. Ng, P. A. Lee, and K. T. Law, Selective equal-spin andreev reflections induced by majorana fermions, *Phys. Rev. Lett.* **112**, 037001 (2014).
- [80] M. Roig, Y. Yu, R. C. Ekman, A. Kreisel, B. M. Andersen, and D. F. Agterberg, Quasisymmetry-constrained spin ferromagnetism in altermagnets, *Phys. Rev. Lett.* **135**, 016703 (2025).
- [81] N. Read and D. Green, Paired states of fermions in two dimensions with breaking of parity and time-reversal symmetries and the fractional quantum hall effect, *Phys. Rev. B* **61**, 10267 (2000).
- [82] N. Nagaosa, J. Sinova, S. Onoda, A. H. MacDonald, and N. P. Ong, Anomalous hall effect, *Rev. Mod. Phys.* **82**, 1539 (2010).
- [83] L. Fu, Topological crystalline insulators, *Phys. Rev. Lett.* **106**, 106802 (2011).
- [84] S. Zeng and Y.-J. Zhao, Description of two-dimensional altermagnetism: Categorization using spin group theory, *Phys. Rev. B* **110**, 054406 (2024).
- [85] K. S. Novoselov, A. Mishchenko, A. Carvalho, and A. H. Castro Neto, 2d materials and van der waals heterostructures, *Science* **353**, aac9439 (2016).
- [86] Y. Ando and L. Fu, Topological crystalline insulators and topological superconductors: From concepts to materials, *Annual Review of Condensed Matter Physics* **6**, 361–381 (2015).
- [87] R. H. McKenzie, Similarities between organic and cuprate superconductors, *Science* **278**, 820–821 (1997).
- [88] K. Miyagawa, K. Kanoda, and A. Kawamoto, NMR Studies on Two-Dimensional Molecular Conductors and Superconductors: Mott Transition in κ -(BEDT-TTF)₂ X, *Chemical Reviews* **104**, 5635 (2004).